Synthetic Dual-Acting Small-Molecule Inhibitors That Target Mycobacterial DNA Replication

Meenakshi Singh*, Stefan Ilic*, Benjamin Tam*, Yesmin Ben-Ishay, Rikeshwer Prasa Dewangan, Dror Sherf, Doron Pappo, Barak Akabayov*

Department of Chemistry, Ben-Gurion University of the Negev, Beer-Sheva, 8410501 Israel

* Correspondence should be addressed to B.A. (akabayov@bgu.ac.il)

***Mycobacterium Tuberculosis* (*Mtb*) is a pathogenic bacterium that is the causative agent of tuberculosis (TB) that kills more than 1.5 million people worldwide annually. One of the main reasons for this high mortality rate is the evolution of new *Mtb* strains that are resistant to available antibiotics. Therefore, new therapeutics for TB are in constant demand. It is known that DNA replication enzymes of *Mtb* and humans are different and this represents a potential target for anti-*Mtb* drug development.**

Here we report the development of potent inhibitors that target simultaneously two DNA replication enzymes of *Mtb*, namely DnaG primase and DNA gyrase, which share a conserved fold near the inhibitors' binding site. In order to improve the physicochemical properties, the binding affinity and inhibitory activity against these two enzymes, 49 novel compounds were synthesized as potential drug candidates in three stages. The last stage of chemical optimization yielded two novel selective inhibitors that exhibit bacteriostatic activity against *Mycobacterium smegmatis* (*Msmg*), a fast growing non-pathogenic model specie of *Mycobacteria*. Efficacy was improved upon conjugation of the best candidate to a cell penetrating peptide (CPP). The inhibitors also impair the development of biofilm, indicating a therapeutic potential of these molecules against infections caused by planktonic and sessile forms of mycobacterium species.

Mycobacterium tuberculosis, DnaG primase, DNA gyrase, Small-molecule inhibitors

Mycobacterium tuberculosis (*Mtb*) is a Gram-positive pathogenic bacterium that is the causative agent of tuberculosis (TB) which infects a third of the world's population. It is the second most prevalent killer, after HIV, among single infectious agents world-wide (World Health Organization, May 2018). New strains of *Mtb* that are resistant to all known classes of antibiotics today pose a global healthcare threat [1].

Replication of the chromosome in *Mtb*, as in other bacteria, is a central event in the cell cycle, performed by a multi-enzyme complex called the replisome. During DNA replication, DnaB helicase unwinds double-stranded DNA and exposes two individual strands [2]. These DNA strands are copied continuously at the leading strand and discontinuously at the lagging strand. On the lagging strand DnaG primase acts to synthesize short RNA primers that mark the starting points of "Okazaki fragments" synthesis by DNA polymerase III holoenzyme. The process of DNA unwinding by DnaB helicase causes twisting tension increase at the coiled portion of DNA as the replication fork advances. This tension interferes with further unwinding of the double-stranded DNA. To prevent this tension on the DNA, Gyr, a type II topoisomerase, acts by creating a transient double-stranded DNA break. It catalyzes negative supercoiling of DNA at the expense of ATP hydrolysis [3]. Both, DnaG primase and GyrB are essential for viability, and have different structural and functional settings in humans (Fig. 1a), thereby providing attractive candidates for antibiotic targeting [4].

Bacterial DnaG-type primases as well as type IA and type II topoisomerases (including Gyr) belong to the same enzyme superfamily based on the presence of a conserved TOPRIM fold within their sequence [5] (Fig. 1b, 1c). This fold consists of approximately 100 amino acids and includes two motifs, one containing a very conserved glutamate residue in its center, whereas the other involves two conserved aspartates (DxD motif, Fig. 1b) [5]. The two conserved motifs have an important role in both primases (e.g. nucleotide polymerization) [6] and topoisomerases (e.g. strand cleavage and rejoining, DNA binding, metal coordination) [7]. It is therefore expected that inhibitors designed specifically for DnaG may inhibit Gyr and vice versa. Coumarin is an example of an inhibitor that binds to the TOPRIM fold of GyrB [8] that was independently discovered to be an inhibitor for *Mtb* DnaG using high throughput screening [9].

Unlike DnaG which serves as a novel drug target, Gyr presents a validated target for anti-tubercular drug discovery. Fluoroquinolones that stabilize the DNA-gyrase complex and promote genomic DNA cleavage [10], along with other Gyr inhibitors, such as novobiocin, are clinically proven as antibacterial agents [11-13]. In addition, resistance to fluoroquinolones (e.g. moxifloxacin and gatifloxacin) remains uncommon in clinical isolates of *Mtb* [14].

New drugs for non-replicating *Mtb*, dormant-like state, are in constant demand [15]. The non-replicating phase can yield formation of biofilm [16], therefore inhibitors designed to halt DNA replication can affect the biosynthesis of biofilm [17]. Small-molecules that inhibit biofilm formation were developed as agents that target non-replicating *Mycobacteria* [18]. Biofilms have been shown to resist penetrability of antibacterial agents [19]. Agents that target DNA replication but can also inhibit biofilm formation could therefore provide new insight into the link between DNA replication and biofilm formation.

A variety of techniques were used to find small molecule inhibitors for DNA replication proteins. A method that combines NMR-fragment screening with an optimization using virtual screening (FBVS) was developed that selects inhibitors for DnaG-type DNA primase [20,21]. FBVS was found to be an effective method especially for challenging targets such as DNA primase [4,22]. This method yielded five small molecule inhibitors that target T7 DNA primase through a similar binding mechanism as shown by high field NMR [21]. Herein, we describe a further development of novel small molecule inhibitors that target *Mtb* DnaG based on the molecules that were found to inhibit T7 DNA primase. Some of these molecules also inhibit Gyr, through binding to common structural features shared by these two enzymes. Derivative molecules were synthesized using medicinal chemistry approaches, two of which were found to inhibit growth of *Msmg* in planktonic and sessile forms (biofilm), thus offering hope for further drug development against TB.

Results

Small molecules that inhibit T7 DNA primase also inhibit *Mtb* DnaG

Using FBVS we found five drug-like molecules, derived from indole and 2H-chromene, that inhibit the primase domain of gene 4 protein of bacteriophage T7 (T7 DNA primase) [21]. The precise binding site of the three molecules (one containing 2H-chromene and two containing indole) within the T7 DNA primase was discovered by high field NMR spectroscopy [21]. T7 DNA primase shares high structural homology with bacterial DnaG primases and therefore it was used as a model target for the development of anti-DnaG small-molecule inhibitors [4]. On a DNA template containing the primase recognition site, DnaG catalyzes the synthesis of RNA primers (Fig. 2a). The ability of *Mtb* DnaG to synthesize oligoribonuceoltides in the presence of small molecule inhibitors was examined. The reaction involved incubating the *Mtb* DnaG with oligonucleotide template (5'- CCGACCCGTCCGTAATACAGAGGTAATTGTCACGGT - 3'),

each one of the four rNTPs, and [α–^{32}P]–ATP. The radioactivity labeled RNA products were separated by denaturing gel analysis and visualized on an autoradiogram (Fig. 2a). The decrease in the radioactive signal strength, which is directly proportional to the amount of synthesized RNA primers, indicates the inhibition of primase activity. Not surprisingly, two of the five inhibitors we found, 3-(2-(ethoxycarbonyl)-5-nitro-1H-indol-3-yl)propanoic acid (Compound **13**) and 7-nitro-1H-indole-2-carboxylic acid (Compound **17**) that inhibit T7 DNA primase, also inhibit the RNA primer synthesis of *Mtb* DnaG (Fig. 2b, lanes 13 and 17).

Few inhibitors for *Mtb* DnaG cross-interact with Gyr of *Mtb* (*Mtb* Gyr)

The compounds found to inhibit DnaG primase were also tested against *Mtb* Gyr that shares a conserved TOPRIM fold with DNA primase. Two assays, ATP hydrolysis and DNA supercoiling assay were carried out with *Mtb* Gyr (Fig. 2b). Upon incubation of *Mtb* Gyr with DNA and [γ–^{32}P]– ATP a radioactive P_i is formed that remains free in solution after treatment with active charcoal. In the presence of a small-molecule inhibitor the decrease in the amount of $^{32}P_i$, indicating a decrease in ATP hydrolysis by *Mtb* Gyr, is quantified using a scintillation counter (Fig. 2b, top panel).

The effect of small molecule inhibitors on the formation of cleavable-complex species by *Mtb* Gyr was also measured. In the presence of ATP and absence of inhibitor the enzyme shows marked DNA relaxation activity characterized by negative supercoiling on pBR322 DNA (Fig. 2b, bottom panel). Inhibition of supercoiling activity is characterized by the appearance of ladder of gel bands (Fig. 2b, bottom panel).

Comparison of all measured activities places the best inhibitor in the bottom left corner of each correlation map (Fig. 2c, Gyr: ATPase vs. supercoiling and primase vs. each Gyr activity). Some of the small-molecules (**13**, **15** and **17**) that were found to reduce [^{32}P]–P_i release (ATP hydrolysis) also inhibit supercoiling of pBR322 DNA by *Mtb* Gyr (Fig. 2c, top-left). Two of the molecules (**13** and **17**) that were found as best inhibitors for *Mtb* DnaG and Gyr contained the indole scaffold substituted with carboxyl-containing functional group (carboxylic acid/ester) in position two/three and electron-withdrawing nitrogen group in position five/seven. The higher molecular mass of compound **13** covers larger chemical space with a potential to yield larger binding interface with the protein target, therefore compound **13**, was selected as a precursor for further optimizations.

Preparation of library of derivatives for the inhibition of *Mtb* DnaG, SAR cycles

A library of 49 novel derivatives was synthesized in order to improve inhibition efficacy. Three rounds of optimization led to better pharmacophore (Fig. 3a). The synthesis of ethyl 3-(3-ethoxy-

3-oxopropyl)-1H-indole-2-carboxylate derivatives (**3a-g**, **3c'**, **4a**, **5a**, **6a-g**, **6c'**, **7a**, **8a-f**, **8c'**, **9a-f**, **9c'**) and the N-benzylated derivatives of ethyl 3-(3-ethoxy-3-oxopropyl)-1H-indole-2-carboxylate (**10a-f**, **10c'**, **11a-f**, **11c'**, **12a-f**, **12c'**, **13a-f** and **13c'**) is depicted in Fig. S1. The synthesis commenced by Japp-Klingemann condensations of the commercially available aniline derivatives **1a-g**, afforded the corresponding diethyl derivatives of phenylhydrazones (**2a-g**) in moderate to good yields. Subsequent Fischer indole cyclisation of the latter phenylhydrazones (p-toluenesulfonic acid, benzene, reflux) [23], produced the key indole derivatives (**3a-g**, **3c'**) in 15–80% yields. Hydrolysis of the latter diesters under mild basic conditions (0.01M NaOH) gave a mixture of the corresponding dicarboxylic acid derivatives **6a-g**, **6c'** (Round I, Fig 3a) and mono-carboxylic acid derivatives **8a-f**, **8c'**, **9a-f**, **9c'** (Round II, Fig. 3a). Reduction of indole diester **3a** using $LiAlH_4$ (THF, 4 ^oC) produced 3-(5-chloro-2-(hydroxymethyl)-1H-indol-3-yl) propan-1-ol (**4a**) in 50% yield, while selective oxidation of the latter di-alcohol **4a** using PCC afforded dicarboxaldehyde **5a** in 40% yield. Diamide **7a** was prepared in two steps from ester **3a** (0.01M NaOH then aniline, DCC and HoBt, dry DMF) in 60% yield. Benzylation of compounds **3a-f**, **3c'** (BnBr, Cs_2CO_3, DMF) afforded obtaining *N*-benzylindoles **10a-f**, **10c'** (Round III, Fig 3a) in 85-95% yields [24]. Partial hydrolysis of the latter diesters (**10a-f**, **10c'**) under mild basic conditions (0.01M NaOH) led to the formation of the corresponding dicarboxylic and mono-carboxylic acids **11a-f**, **11c'**, **12a-f**, **12c'**, **13a-f**, and **13c'** in low to moderate yields.

The newly synthesized molecules were tested for their ability to inhibit the activities of *Mtb* DnaG and Gyr (Fig. 3b-c). Some of the newly added groups (3-$CF_3$4-Cl and 2-Cl4-CF_3 substituents) were essential for inhibition of primase and Gyr activities (Fig. 3b-c), whereas other functional groups (carboxaldehyde, amide and alcohol substituents) did not improve inhibition (compounds **4a**, **5a**, and **7a**). Summary of SAR conclusions is presented in Fig. 3d. For example, a decrease in potency of compounds **6a-g**, **6c'**, **4a**, **5a**, and **7a** was attributed to the absence of carboxyethyl and propanoic acid groups at position 2 and 3, respectively. Schematic representation of the three rounds of optimization, for each specific aniline derivative (**1a-d**), is shown in Fig. S2. With the new lead structure (compound **8c** and **8d**) in hand, additional substituents were added to the indole moiety to further develop the structure–activity relationship for the Group II series. Introduction of a benzyl group in -NH position of indole ring to Group II series of compounds increased potency dramatically (as noted for the resulting Group III series of compounds).

Out of 49 newly synthesized compounds, nine compounds (**8c**, **8d**, **8f**, **11c'**, **12c**, **13a**, **13b**, **13c**, **13d**) were found to inhibit DnaG primase and Gyr of *Mtb* (Fig. 3b-c) with molecules 3-(1-benzyl-5-chloro-2-(ethoxycarbonyl)-4-(trifluoromethyl)-1H-indol-3-yl)propanoic acid (**13c**) and 3-

(1-benzyl-7-chloro-2-(ethoxycarbonyl)-5-(trifluoromethyl)-1H-indol-3-yl)propanoic acid (**13d**) that present the best inhibitors in all measured activities for DnaG and Gyr of *Mtb* (Fig. 3e). Dose response of selected molecules on the DnaG/Gyr activities is presented in Figs. S3-4. Molecular structure of all molecules was characterized by NMR and MS as presented in SI1.

Some of the inhibitors act to stop proliferation of *Mycobacterium smegmatis (Msmg)*

Since DnaG and Gyr are essential enzymes for every bacterial cell, it seemed likely that compounds **13c** and **13d** would also affect the growth of *Mycobacteria. Msmg* is a nonpathogenic relative of *Mtb*, often used to test antitubercular agents due to the similar morphological and biochemical properties of these two bacterial species. For example, both enzymes used in this study, DnaG primase as well as GyrB subunit, exhibit more than 80% identity between *Mtb* and *Msmg*.

The primase/Gyr inhibitors were screened for inhibition of growth of *Msmg* mc^2155 over a time course of 20h at 37° C. The antibacterial activity of compounds **13c** and **13d** were determined by assaying their minimal inhibitory concentration (MIC) against *Msmg*. The results are summarized in Fig. 4. Both compounds inhibited the growth of *Msmg* in accordance with their inhibition of mycobacterial primase/Gyr. Other compounds that showed inhibition of the two enzymes in vitro had little or no effect against *Msmg* (Fig. 4, growth curve, colored blue). The MIC_{90} of compounds **13c** and **13d** were 86.6 and 250 μM, respectively (Table 1, Fig. 5). This value was even better than the effective dose measured for isoniazide (250 μM), a first-line anti-TB drug and a central drug in the common treatment regimens (Fig. 4a inset-coloured grey and Table 1).

Conjugation of molecules with cell penetrating peptide for increased cellular uptake and potency

A major limitation for antibiotics against intracellular pathogens such as *M. tuberculosis* is the need to cross several biological membranes to access the target site[25]. Furthermore, pathogenic mycobacteria present an intrinsically impermeable thick cell wall, which provides as a robust barrier to most antibiotics [26]. Cellular drug delivery can improve efficacy and potency of hydrophobic molecules (water insoluble) which cannot reach high concentration within the cells. Therefore, the transport of physiologically active compounds across membranes into target cells can be facilitated by cell-penetrating peptides (CPPs), such as HIV-TAT peptides, and octa-arginines[27-29]. It has been previously reported that arginine rich cell penetrating peptide can efficiently deliver the covalently conjugated small molecules into *Mtb*[30]. Here we have

conjugated the biochemically most active molecule from our series, **13d** with two cell penetrating peptides (Fig. 4c): HIV TAT (GRKKRRQRRRPQ-$CONH_2$) and octaarginine (R_8) and evaluated their efficacy against the bacterial growth of *M. smegmatis* as well as their interaction with DnaG/Gyr (Fig. 4-5 and Fig. S5 and Fig. S8). Interestingly, the conjugated molecules were found to be >50 fold active against the *M. smegmatis* mc^2155, compared to compound **13d** alone, with the MIC range of 1.9 – 3.9 μM (Fig. 5 and S5, Table 1). Under identical conditions we also evaluated the antibacterial activity of cell penetrating peptides and MIC was found to be 7.8 μM for both peptides (Table 1). Hence the conjugation of compounds with peptide facilitates the cellular uptake of DnaG inhibitors and synergistically potentiates the antibacterial activity.

Inhibition of biofilm formation of *Msmg*, a phenotype for the inhibition of DNA replication

Previous studies have shown that inhibition of DNA replication affects biofilm formation and stability of preformed biofilm[31]. This link between DNA replication and biofilm formation is likely to be consequential. To determine whether compounds **13c** and **13d** exert their antibacterial effect on biofilm, cells were treated with each compound and their biofilm phenotypes were assessed as described previously[32]. Specifically, the effect of molecules **13c** and **13d** on the formation inhibition and eradication of preformed biofilm of *Msmg* mc^2155, was examined. Initial inoculums of *Msmg* were incubated with their MIC and sub-MIC of all compounds including isoniazid and CPP conjugates. At MIC (250 μM) and sub-MIC (125 μM) concentration compound **13c** inhibited the biofilm formation up to 99% and 98%, respectively, as compared to DMSO control (Fig. 5a). The second compound, **13d**, also inhibited biofilm formation, up to 85 % at its' MIC (250 μM) but was unable to inhibit at half-MIC (125 μM). We also evaluated the effect of peptide conjugated **13d** against biofilm formation at their MIC and sub MIC level and found to inhibit biofilm formation up to >99%. In identical conditions the peptides alone were not able to inhibit the biofilm formation in both concentrations. Surprisingly, in identical conditions the standard drug isoniazid reduced biofilm formation up to 65% at MIC and did not inhibit the biofilm formation significantly at sub-MIC level (Fig. 5a). To further corroborate, the alamar blue cell viability assay was performed and we also counted the CFU from *Msmg* biofilm suspensions treated with our compounds by plating each sample on the 7H10 agar plate (Fig. S5).

To evaluate the ability of these molecules to disrupt biofilm or inhibit pre-formed biofilm of *Msmg* mc^2155 cells we have added the compounds at their respective MIC and sub-MIC to the four days old biofilm and continued the incubation for additional three days. Interestingly, both compounds **13c** and **13d** significantly reduced the preformed biofilms at their MIC level up to

69.28% and 48.48%, respectively (Fig. 5b). At the sub-MIC concentration compound **13c** was not able to eradicate the biofilm, whereas **13d** inhibited significantly the biofilm up to 55.0 % as compared to the DMSO control. Surprisingly, peptide conjugated to **13d** and peptide alone did not affect the preformed biofilm of *Msmg*, whereas isoniazid induced the biofilm formation as reported previously [33].

Discussion

Mtb poses a global health hazard, especially since the emergence of drug-resistant strains. Therefore, new antibiotics with novel mechanisms of action are needed to enrich the current treatment regimens. The DNA replication machinery represents a multiprotein target with very high potential in antibacterial drug design that has been underexploited thus far. Using FBVS we have discovered five small molecule inhibitors for T7 DNA primase that was used as a model system for DnaG-like primases [21]. Not surprisingly two molecules that inhibit T7 DNA primase were also found to inhibit *Mtb* DnaG. High field NMR was used to determine the location of the precursor inhibitor (compound **13**) in the binding site of T7 DNA primase. Aligning the structure of T7 DNA primase (PDB ID: 1nui) [34] with that of *Mtb* DnaG (PDB ID: 5w33) [35] provided some insight into the binding site of the precursor molecule (compound **13**) within *Mtb* DnaG (Fig. S6a). A few molecules also inhibit *Mtb* Gyr, presumably through binding to the conserved TOPRIM fold that Gyr shares with DnaG primase, as suggested after docking to the available structure of *Mtb* Gyr (Fig S6). Since the Toprim fold is the common structural feature between the two enzymes we suggest that this fold might have a role in directing the molecules to their designated binding sites.

Compound **13** that served as a promising inhibitor in the initial screening was chosen as a precursor for optimization. To understand which modifications lead to the increase in potency a systematic set of modifications was performed on this precursor molecule. The effect of each modification was tested by observing the changes in the activities of *Mtb* DnaG and Gyr. Three rounds of optimizations allowed us to draw SAR conclusions related to the inhibitor scaffold.

A few molecules that were found to inhibit DNA primase also inhibit Gyr. Although the IC_{50} values determined for each enzyme remained in the micromolar range, some of the molecules were able to effectively inhibit growth of bacterial culture (*Msmg*), presumably due to a dual mechanism of action (synergistic effect).

Functional group modifications based on structure-activity relationships to identify pharmacophore

In search for new leads affecting DNA replication of *Mtb*, ethyl 3-(3-ethoxy-3-oxopropyl)-1H-indole-2-carboxylate derivatives and their N-benzylated (N-Bn) analogues are reported here as novel synthetically designed inhibitors of *Mtb* DnaG primase and Gyr. The preliminary study with 18 commercial small-molecules, and their inhibitory activity against *Mtb* DnaG primase and Gyr has provided initial insight into the molecular structure required for the development of more potent inhibitors. For example, we have observed that the substituent on the phenyl or indole ring may have a significant effect on the potency of the inhibitor. The presence of strong electron withdrawing groups such as a trifluoromethyl substituent (**13c** and **13d**) on the phenyl ring of the round III series of compounds led to a significant increase in the inhibitory effect compared to the chloro and nitro substituted compounds (**10a** and **10b**), respectively (Null activity). On the other hand, the presence of electron releasing groups, especially methyl group (**3g**), resulted in decreased potency of inhibition compared to compound **3c'**. The reduction of ester function (**3a**) to alcohol group (**4a**) and then oxidation to aldehyde group (**5a**) led to loss of activity. The amide coupling to carboxylic acid derivative (**6a**) gave rise to compound (**7a**), which presented some inhibitory activity on Gyr but not on primase. In order to further explore the effect of N-benzylation of indole on inhibitory activity, compounds (**10a-f**, **10c'**, **11a-f**, **11c'**, **12a-f**, **12c'**, **13a-f** and **13c'**) were synthesized and their efficacies were tested. When the benzyl group was introduced at the NH-position of the indole ring, the inhibitory effects of the resulting compounds increased dramatically in comparison with compounds (**3a-g**, **3c'**, **6a-g**, **6c'**, **8a-f**, **8c'**, **9a-f**, **9c'**). We have concluded that the carboxyethyl group at position 2, an electron withdrawing group on phenyl ring of indole-3-carboxylic acid scaffold, as well as N-benzylation, are important for the biological activity. The representatives of round III compounds have better efficacies than their non-benzylated analogues belonging to round II compounds (**8c** and **8d**). Overall, the N-benzylation of compounds (**3a-g**, **3c'**) gave rise to compounds (**13a-f** and **13c'**), which presented maximum inhibitory activity thus far.

The carbonyl-containing groups in positions 2 and 3 of indole probably act as hydrogen bond acceptors, whereas the N-Bn group can also mediate the π-π stacking interactions with aromatic amino acids present in the predicted binding pocket of *Mtb* DnaG (e.g. tyr-128, tyr-143, phe-149, phe-157, phe-161) (Fig. S6).

Taken together, the SAR studies demonstrated that a variety of hydrophobic substituents introduced on a phenyl ring of indole were well tolerated, and among them the chloro, trifluoromethyl and nitro moiety were preferred. The substituents at position 1 (N-benzyl) as well

as positions 2 and 3 (ester and carboxylic acid respectively) of indole were proven to be important for inhibitory activity. In view of our results, it is rationally presumed that the best inhibitors for *Mb* DnaG/Gyr (**13c** and **13d**) present a viable template to discover more potent inhibitors, by variations of substituents on the phenyl ring or -NH of indole.

The activity and potency of best analogs 13c and 13d is modulated by tight interactions between the pharmacophore and the targets' amino acid residues

Functional group modifications can change the specificity and binding affinity of the molecule to the target's binding site. Some structural variations in the molecules may allow SAR continuity that results in an increased potency. On the other hand, discontinuity in SAR that markedly reduces the potency of an inhibitor after a small chemical modification is termed "the functional cliff". A demonstration for a functional cliff is presented in Fig. 6, where three sub-structures that construct compounds **10c** and **10d**, and their corresponding analogues **13c** and **13d**, are defined (Fig. 6, region A-blue, region B-red, and region C- green). The compounds **10c** and **10d** present null biological activity (ability to inhibit DnaG and Gyr from *Mtb*) although they share similar structure with compounds **13c** and **13d** (Fig. 3d). Therefore, we conclude that the addition of 3-$CF_3$4-Cl (**13c**) and 2-Cl4-CF_3 (**13d**) substituents (region B) to compounds **10c** and **10d** is essential for improving the inhibitory activity against DnaG and Gyr. In addition, introduction of a benzyl group on the pharmacophore (region C) increases the potency of the compounds. Importantly, when the ester group was replaced with a carboxylic acid moiety in region A (position 3), the molecules (**13c** and **13d**) were more active both in enzymatic and bacterial assays (Figs. 3-4), indicating that the presence of carboxyethyl and propanoic acid group at position 2 and 3, respectively, is important for an extended interaction with the primase/Gyr. The increase in potency upon modifications of region C and of the distal parts of region B, whereas modifications of region A reduced potency, indicate that region A is the most important functional group of the pharmacophore.

CPP conjugates were used as a strategy for increasing intra-bacterial intake of the small molecule inhibitors. Although the peptide alone is toxic to the cells, small molecule conjugate exhibited higher toxicity presumably through additional mechanism mediated by electrostatic interactions with the DNA (Fig. S8). More specifically, the small molecule serves to anchor the peptide to the protein target, whereas the peptide itself, due to its positive charge, may prevent interaction of DnaG/Gyr with negatively charged DNA. In addition, inhibition of DNA replication by small molecule conjugates also affects biofilm formation. It is possible that inhibitors that halt

DNA replication hamper communication between *Msmg* cells and inhibit their biofilm formation or even eradicate preformed biofilms. We therefore suggest that our DNA replication inhibitors can target planktonic resistance of *Mycobacteria*.

Online Materials and Methods

Materials

All chemicals and solvents used for the synthesis and characterization of compounds were purchased from Sigma-Aldrich and Acros, and were of reagent grade without purification or drying before use. Chemicals used for biochemical assays were molecular-biology grade, purchased from Sigma-Aldrich. Ribonucleotides (ATP, CTP, GTP and UTP) were purchased from New England Biolabs (NEB). [α–^{32}P] ATP (3000 Ci/mmol) and [γ–^{32}P] ATP (3000 Ci/mmol) were purchased from Perkin Elmer. ^{1}H NMR data were recorded on a 400/500 MHz Bruker NMR instrument, and ^{13}C NMR data were recorded on a 101 MHz Bruker NMR instrument. Chemical shifts were reported in δ (ppm) downfield from tetramethylsilane (TMS) and were recorded in appropriate NMR solvents ($CDCl_3$, δ 7.26; CD_3OD, δ 3.31; $(CD_3)_2CO$, δ 2.05; or other solvents as mentioned). All coupling constants (J) are given in Hertz. All of the NMR spectra were processed by MestReNova software (www.mestrelab.com). The following abbreviations are used: s, singlet; d, doublet; t, triplet; m, multiplet; br s, broad singlet peak. Mass spectra were recorded only for the molecules that exhibited best activity, using an HRMS instrument. Thin layer chromatography (TLC) was performed on Merck aluminum backed plates, pre-coated with silica (0.2mm, 60F254) and the detection of molecules was performed by UV fluorescence (254 nm). Column chromatography separations were performed using silica gel (0.04-0.06 mesh) as stationary phase.

All the Fmoc protected amino acids and N,N,N′,N′-Tetramethyl-O-(1H-benzotriazol-1-yl)uronium hexafluorophosphate (HBTU) were purchased from Novabiochem and G.L. Biochem (Shanghai) Ltd. N,N,-Dimethylformamide (DMF) and dichloromethane (DCM) was purchased as biotech grade from Avantor J.T. Baker. Analytical HPLC was performed on a Dionex 1100 using a reverse phase C18 column at a flow rate of 1.5 mL/min. Preparative HPLC was performed on a Dionex Ultimate 3000 instrument using a C18 reverse phase preparative column at a flow rate of 20 mL/min. Mass spectrometry analysis was performed by LC-MS Thermo Surveyor 355.

Proteins expression-purification

DnaG primase from *Mtb*

The DNA sequence encoding DnaG primase from *Mtb* H37Rv was cloned into pET28 vector. *Escherichia coli* BL21 (DE3) cells were transformed with created expression vector, grown in LB medium containing 50 mg/mL kanamycin until OD_{600} = 0.7 and induced with 0.5 mM IPTG. After induction, the culture was incubated with shaking for 4h at 37°C. Cells were harvested by centrifugation (4700 x g, 15 minutes) and pellet was resuspended in the lysis buffer (50 mM Tris-HCl pH 7.5, 500 mM NaCl, 10% v/v glycerol, and 1 mM dithiothreitol). Lysis was performed using pressure homogenizer. The lysate was clarified by centrifugation (21000 x g, 30 minutes), filtered through 0.45 µM filter and loaded onto Ni-NTA column (HisTrap FF, GE Healthcare). The column was equilibrated with buffer A (50 mM Tris-HCl pH 7.5, 500 mM NaCl, 10% v/v glycerol, 1 mM dithiothreitol and 10 mM imidazole) and the protein was eluted with a linear gradient of imidazole (10-500 mM) in buffer A. The fractions containing Mtb DnaG primase were joined and EDTA was added to a final concentration of 1 mM. Ammonium-sulfate was added (0.4 g/mL of sample) with stirring and left for several hours at 4ºC to precipitate the protein. Centrifugation was performed (21000 x g, 30 minutes) and the protein precipitate was dissolved in buffer C (50 mM Tris-HCl pH 7.5, 500 mM NaCl, 10% v/v glycerol, 1 mM dithiothreitol, 1 mM EDTA) and loaded onto Superdex S200 column (GE Healthcare). The protein was eluted in buffer C. Fractions containing purified Mtb DnaG primase were joined and dialyzed against buffer C containing 50% glycerol. The protein samples were stored at -20 ºC.

Gyrase

Mtb Gyr subunit A and B were purified separately. The DNA sequences encoding each Gyr subunit from *Mtb* H37Rv were cloned into separate pET28 vectors. *Escherichia coli* BL21 (DE3) AI cells were transformed with created expression vectors, grown in LB medium containing 50 mg/mL kanamycin until OD_{600} = 0.6 and induced with 0.5 mM IPTG and 0.2% arabinose. After induction, the culture was incubated with shaking for 4h at 30 °C. Cells were harvested by centrifugation (4700 x g, 15 minutes) and the pellet was resuspended in buffer A (50 mM Tris-HCl pH 8, 500 mM NaCl, 10 mM imidazole, 10% v/v glycerol, and 0.5 mM dithiothreitol). Lysis was performed using pressure homogenizer and sonication. The lysate was clarified by centrifugation (21000 x g, 60 minutes), filtered through 0.45 µM filter and loaded onto Ni-NTA column (HisTrap FF, GE Healthcare). The column was equilibrated with buffer A and the protein was eluted with a linear gradient of imidazole (10-400 mM) in buffer A. The fractions containing Mtb Gyr were joined and concentrated by dialysis against buffer B (20 mM Tris-HCl

pH 8, 100 mM NaCl, 50% v/v glycerol, and 2 mM dithiothreitol) and loaded onto Superdex S200 column (GE Healthcare) The column was equilibrated and the protein was eluted with buffer C (20 mM Tris-HCl pH 8, 500 mM NaCl, 10% v/v glycerol, and 1 mM dithiothreitol). The fractions containing purified *Mtb* Gyr were joined and dialyzed against buffer B and stored at -20 ºC.

Oligoribonucleotide synthesis assay by *Mtb* DnaG primase

Standard 10 µL reaction contained 50 µM of DNA template (5'-CCGACCCGTCCGTAATACAGAGGTAATTGTCACGGT-3'), 250 µM GTP, CTP, UTP and [α-^{32}P]-ATP, and *Mtb* DnaG primase in a buffer containing 40 mM Tris-HCl (pH 7.5), 1 mM $MnCl_2$, 10 mM DTT, and 50 mM KGlu. After incubation at 37ºC for 60 minutes with the inhibitor, the reaction was terminated by adding an equal volume of sequencing buffer containing 98% formamide, 0.1% bromophenol lblue, and 20 mM EDTA. The samples were loaded onto a 25% polyacrylamide sequencing gel containing 7 M urea, and visualized by autoradiography.

DNA supercoiling assay for *Mtb* Gyr

DNA supercoiling activity was tested with purified *Mtb* GyrA and GyrB subunits mixed in 2:1 ratio. The reaction mixture contained 50 mM HEPES [pH 7.9], 100 mM potassium glutamate, 6 mM magnesium acetate, 2 mM spermidine, 4 mM dithiothreitol, 50 µg/ml bovine serum albumin, 1 mM ATP and 13.34 ng/µl relaxed pBR322 DNA, and small molecules in appropriate concentrations (10% V/V DMSO final). One unit of Gyr proteins was added (one unit of enzyme activity was defined as the amount of Gyr that converted 400 ng of relaxed pBR322 to the supercoiled form in 1 h at 37°C in 30 µl reaction), and the reaction mixtures were incubated at 37°C for 1 h. Reactions were terminated by adding one reaction volume of Stopping Buffer (40% sucrose, 100 mM Tris-HCl pH 8, 10 mM EDTA, 0.5 mg/ml Bromophenol Blue) and two reaction volumes of chloroform/isoamyl alcohol (v:v, 24:1). The samples were vortexed, centrifuged briefly and loaded onto 1% agarose gel in 1X Tris-borate- EDTA buffer, pH 8.3 (TBE). Electrophoresis was performed for 4h at 40 V, and the gel was subsequently stained with ethidium bromide (0.5 mg/ml).

ATPase Norit assay for *Mtb* Gyr

The standard assay for ATPase measures the formation of Norit-adsorbable ^{32}P-labeled phosphate arising from the hydrolysis of [γ-^{32}P]-ATP. ATPase assay was carried out according to the same reaction conditions as for DNA supercoiling except that 170 nM [γ-^{32}P]-ATP (30 cpm/pmol) was used instead of non-radioactive 1 mM ATP. The reaction mixture (10 µl) was incubated at 37 °C for 60 minutes. The reaction was stopped by the addition of 90 µl of a

solution consisting of 0.6 ml of 1 M HCl, 0.1 M $Na_4P_2O_7$, 0.02 M KH_2PO_4, 0.2 ml of a Norit A suspension (20% packed volume), and 0.1 ml of bovine serum albumin (5 mg/ml). The solutions were mixed and allowed to sit for 5 min at 0 °C. After centrifugation, 10 µl of the supernatant was spotted in a scintillation tube and upon the addition of Ultima Gold scintillation liquid (Perkin Elmer) the signal was measured by scintillation counter.

Bacterial growth assay

Bacterial strains and growth media

Msmg cells mc^2155 (wild type), containing Hygromycin resistance gene and transcriptional red fluorescent protein gene (mCherry), were grown in Middlebrook 7H9 broth (Fluka) liquid medium supplemented with glycerol (0.4%, v/v) and Tween-80 (0.05%, v/v) (7H9++ liquid medium). Solid medium was composed of Middlebrook 7H10 agar (Difco) and 0.4% (v/v) glycerol (7H10+ agar solid medium). Hygromycin was added to both liquid and solid media to a final concentration of 50 µg/mL. The experiments were conducted under strictly sterile conditions. All instruments, materials and mediums involved were sterilized before use. Experimental procedures were performed in a biological hood with a laminar flow.

Bacterial growth of *Msmg* culture

Msmg culture was first inoculated onto 7H10+ agar plate (medium components are described above) containing 50 µg/mL hygromycin and incubated at 30ºC for approximately four days. The primary liquid culture was prepared by transferring numerous colonies from a previously inoculated 7H10+ agar plate into 10 mL of 7H9++ liquid medium containing 50 µg/mL hygromycin. Cells were incubated overnight (~16 hours) at 30 ºC with shaking (200 rpm). The secondary culture was prepared by transferring 1 mL of *Msmg* primary culture into 50 mL 7H9++ liquid medium (1:50 ratio, v/v) supplemented with 50 µg/mL hygromycin. Again, cells were grown overnight at 30 ºC with shaking (200 rpm) to mid-log phase (OD_{600} ~0.5). Then the culture was diluted to OD_{600} = 0.025, dispensed in wells of Thermo Scientific™ Nunc™ F96 MicroWell™ black polystyrene plate and treated with different small molecule inhibitors at concentration of 250 µM. The plate was incubated at 30°C with continuous orbital shaking (567 cpm) over the course of 20 hours. The cell growth was monitored simultaneously by Synergy H1 microplate reader (Biotek) using mCherry as a reporter protein (mCherry fluorescent signal directly correlates with the number of live bacterial cells). Data represents the average of three biological replicates (n=3).

Dilution colony assay (*Msmg* colonies)

The samples from the previously described procedure (Bacterial growth of Msmg culture) were also used for dilution colony assay as explained in the following text. After two hours of monitoring the bacterial growth in Synergy H1 microplate reader, 3µL of each sample was collected and serially diluted in 1:10 ratio ($x10^{-1}$, $x10^{-2}$,$x10^{-3}$, $x10^{-4}$). Then 3 µL of each dilution was transferred onto 7H10+ agar plate and incubated at 30°C for four days or until clear colonies were observed in the positive control sample (sample that didn't contain any inhibitor).

Inhibition of biofilm formation of *Msmg*, a phenotype for the inhibition of DNA replication

Msmg mc2155 were routinely cultured in Middlebrook 7H9 media (4.7 gm/L) supplemented with 0.2% v/v glycerol and 0.05% v/v Tween 80 and grown at 30°C with shaking at 125 rpm for 48 h. For biofilm inhibition assay, the previously reported protocol was used [32] with slight modifications. Briefly, freshly grown *Msmg* mc2155 was diluted in fresh biofilm growth media (Middlebrook 7H9 media with 0.2 % glycerol supplemented with 0.5% glucose) 100 times (100 µl culture was diluted in 10ml of media). 500 µl of diluted culture was dispensed in wells of a 48-well polystyrene plate for biofilm formation. To evaluate the inhibition of biofilm formation, compounds **13c**, **13d** (stock solution of 20 mM in DMSO) and isoniazid at 250 µM and 125 µM concentrations were added initially with diluted culture. Final concentration of DMSO in culture was 2.5% v/v in each well and only 2.5% DMSO was used in a control sample. The plate was sealed with parafilm and incubated at 37 °C in incubator for five days without shaking. After five days of incubation 0.1% Tween 80 was added to each well and gently swirled to dissolve the detergent. After 15 minute of incubation pellicles were collected and washed thrice with PBS containing 10% glycerol and 0.05% Tween 80. Pellicles were kept on rocker at 4 °C for 12 h in the same buffer for dispersal of matrix. Suspension was then homogenized by vortexing, diluted ten times in buffer and 90µl of each sample was dispensed into 96 well polypropylene plates. 10 µl of alamar blue reagent was added in each well to check the viability of bacterial cells. Plate was further incubated at 37 °C for 8h and percentage reduction of alamar blue was calculated by measuring fluorescence at excitation wavelength of 570nm and emission wavelength of 600nm. To further corroborate and validate the result of alamar blue assay the bacterial suspensions were diluted 10 times in PBS and 10 µl of each suspension was plated on a MH10 agar plate in order to count colony forming units (CFU).

In silico molecular docking

Molecular docking simulations were performed using AutoDock 4.2 [36] in order to estimate the binding free energy (ΔG_{bind}), and the positions of the investigated compounds within the receptor. The simulations were performed by using available crystal structure of *Mtb* DnaG (PDB ID: 5W33) and Mtb Gyrase subunit B (PDB ID: 5BS8). Cognate ligands chosen for this purpose included two of the most active newly synthesized inhibitors (**13c** and **13d**). Both the receptor and ligand molecules were preprocessed for docking according to the AutoDock user manual. A docking grid was set with 126 points in each dimension and a default spacing of 0.375 Å. The received grid map was centered with respect to the receptor. Free energy calculations and conformational sampling of the ligands were then carried out through Lamarckian genetic algorithm (LGA), with an initial population size of 150 individuals, 2,500,000 free energy evaluations and 27,000 LGA generations. Clustering of the results was performed *via* root mean-square deviation (RMSD) calculations for the obtained poses of the ligands, with a constant tolerance of 2.0 Å.

Synthesis of indole derivatives

Scheme for the synthesis of all molecules below is presented in Fig. S1

A. General procedures for the synthesis of compounds (2a-g).

(i) *Preparation of benzenediazonium salt derivatives (mixture I).* To a well stirred solution of aniline derivatives 1a-g (10 mmol) in 5M aq. HCl (16 ml) at 0°C was added dropwise a cold solution (0–5°C) of sodium nitrite (1.38 g, 20 mmol, 2 equiv.) in 10 ml water. Slow addition rate was kept in order to maintain the reaction temperature at 0°C. The resulting mixture was stirred at 0–5°C for additional 30 min in an ice bath.

(ii) *Preparation of 2-(ethoxycarbonyl)cyclopentanone anion (mixture II).* A solution of 2-(ethoxycarbonyl)cyclopentanone (2.512 ml, 1.344g, 15 mmol) in ethanol (5 ml) was cooled to 0–5°C. Then, a potassium hydroxide solution (5.040 g, 90 mmol, 6 equiv.) in water (5 ml) previously cooled to 0–5°C was added dropwise over a period of 30 min in order to keep the reaction temperature below 8°C. The white-milky appearance mixture was stirred for further 30 min at 0–5°C.

(iii) *Preparation of monoethyl derivatives of phenylhydrazones (mixture I+ mixture II).* Ice (50 g) was added to mixture II with stirring at 0–5°C in an ice bath, followed by the addition of mixture I, and stirring continued for 1 h at 50°C. The combined mixtures were brought to room temperature and the pH was subsequently adjusted to 4–5 with 1 M aq. HCl. The mixture was extracted with diethyl ether (50 ml×3) and the combined organic layer was dried over

magnesium sulfate and filtered. The volatiles were removed under reduced pressure affording a gummy material (95–100%) that was used without further purification in the next step.

(iv) *Preparation of diethyl derivatives of phenylhydrazones (2a-g).* Concentrated H_2SO_4 (2.7 ml, 50.5 mmol, 5.1 equiv.) was added dropwise to a stirred solution of monoethyl derivatives (10 mmol) in absolute ethanol (100 ml). The reaction mixture was then heated to reflux for 3 h at 100°C. Then the ethanol was removed under reduced pressure and the residue was treated with 100 ml of ice water. The aqueous solution was extracted with dichloromethane (3 X 50 ml). The combined organic layer was dried over magnesium sulfate, filtered and concentrated. The residue was purified by silica gel column chromatography (ethyl acetate:hexane, 1:4) led to the desired product in 80–95% yield as a yellow/brown solid.

B. General procedures for the synthesis of ethyl 3-(3-ethoxy-3-oxopropyl)-1H-indole-2-carboxylate derivatives (3a-g, 3c').

A mixture of p-toluenesulfonic acid (3.800 g, 20 mmol, 4 equiv.) and 100 ml of benzene was refluxed for 2 h at 110°C under azeotropic condition. Subsequently, 5 mmol of diethyl derivatives of phenylhydrazone (**2a**–**g**) was added and the mixture refluxed for 24 h before the volatiles were distilled. The mixture was washed with saturated solution of $NaHCO_3$ (2 X 30 ml) and water (30 ml). The crude reaction mixture was extracted with dichloromethane (3 X 30 ml) and then washed with water (3 X 20 ml). The organic layer was dried over magnesium sulfate, filtered, and concentrated under reduced pressure. The residue was purified by silica gel column chromatography using ethyl acetate/hexane (1:9 to 1:6) as eluent producing pale white/yellow solid in 15–80% yield.

C. Synthesis of compound 4a.

Dry THF (20 ml) was added dropwise under N_2 atmosphere to an ice-cooled RBF containing $LiAlH_4$ (342 mg, 9.0 mmol, 6 equiv.) at 0°C. After completion of THF addition, conc. H_2SO_4 (240 µl, 4.5 mmol, 3 equiv.) was added to the reaction mixture and the resulting mixture was left to stir at 0°C for 30 min. To the stirred reaction mixture, compound 3a (1.5 mmol) in dry THF was slowly added within 30 min at 0°C and the resulting mixture was left to stir at room temperature for 2 h. After completion of the reaction, ice was added to the resulting reaction mixture and was filtered. Filter cake was washed with ethyl acetate (3 X 20 ml) and then with water (3 X 10 ml). The organic phase was collected, dried over magnesium sulfate and filtered. Solvent was removed under vacuum to produce grey solid. The residue was purified by silica gel column

chromatography using methanol/dichloromethane (1:19) as eluent led to the final products in 50% yield as grey-white solid.

D. Synthesis of compound 5a.

To the solution of compound **4a** (0.05 mmol) in dry DCM (5 ml) was added PCC (32 mg, 0.15 mmol, 3 equiv). The reaction mixture was stirred for 3h at room temperature. After completion of the reaction, powdered $MgSO_4$ was added to the resulting reaction mixture and then anhydrous ether (5 X 5 ml) was added, 5X of reaction solvent. The reaction mixture was then, filtered and concentrated. The residue was purified by silica gel column chromatography using ethyl acetate/hexane (1:4) as eluent led to the desired product in 40% yield as a pale white solid.

E. Synthesis of compound 7a.

HOBt (25mg, 0.16 mmol, 2 equiv.) was added to a stirred solution of compound **6a** (0.08 mmole) in dry DMF (10 ml) under N_2 atmosphere. Subsequently, solution of aniline (15mg, 0.16 mmol, 2 equiv.) in dry DMF was added to the reaction mixture followed by the addition of DCC (34mg, 0.16 mmol, 2 equiv.) and DIPEA (5% equiv.). The resulting mixture was left to stir at room temperature for 48 h. After completion of the reaction, reaction mixture was washed with 1M HCl (3 X 15 ml) followed by 0.1M Na_2CO_3 aqueous solution (3 X 20 ml) to quench the reaction. The crude mixture was extracted with ethyl acetate. The organic layer was then washed with brine (3 X 15 ml), dried over magnesium sulfate, filtered, and evaporated to dryness. The residue was purified by silica gel column chromatography (ethyl acetate:hexane, 1:6) as eluent led to compound 7a in 60% yield as a white solid.

F. General procedures for the synthesis of compounds (6a–g, 6c'), (8a-f, 8c'), (9a-f, 9c') and (11a–f, 11c'), (12a-f, 12c'), (13a-f, 13c').

Compound **3a–g, 3c'** (0.5 mmol) and **10a-f**, **10c'** (0.5 mmol) were dissolved in 50 ml tetrahydrofuran (THF) and the mixture stirred at room temperature for 1 h. Then a solution of NaOH (0.01M) was added and the reaction stirred at room temperature for 18-24 h. After completion of the reaction, the pH was adjusted to 2–3 using 1M aq. HCl, and the product was extracted with diethyl ether (3 X 20 ml). The combined organic layer was dried over magnesium sulfate, filtered, and evaporated to dryness. The residue was purified by silica gel column chromatography (ethyl acetate/hexane, 1:10 to 1:5) as eluent affording products **6a–g**, **6c'**, **8a-f**, **8c'**, **9a-f**, **9c'** as well as **11a–f**, **11c'**, **12a-f**, **12c'** and **13a-f**, **13c'** in as white solids.

G. General Procedures for the Synthesis of N- benzylated derivatives of ethyl 3-(3-ethoxy-3-oxopropyl)-1H-indole-2-carboxylate (10a-f, 10c').

A catalytic amount of KI (8 mg, 0.05 mmol) and benzyl bromide (214 mg, 1.25 mmol, 2.5 equiv) were added to stirred solution of compounds **3a-f**, **3c'** (0.5 mmol) and Cs_2CO_3 (488 mg, 1.5 mmol, 3 equiv) in DMF (20 ml). The reaction mixture was heated to 60°C for 2 h, and then concentrated under vacuum. The residue was dissolved in EtOAc (25 ml), washed with water (3 X10 ml), dried with anhydrous $MgSO_4$ and concentrated under reduced pressure. The crude product was purified by silica gel column chromatography (ethyl acetate/hexane, 1:9) as eluent affording compounds **10a-f** and **10c'**) in high yields (85-95%) as yellow oils.

Preparation of cell penetrating conjugates

The Fmoc based solid phase peptide synthesis strategy was used for the synthesis of TAT peptide (GRKKRRQRRRPQ-$CONH_2$) and octaarginine (NH_2-RRRRRRRR-$CONH_2$) on Rink amide MBHA resin by using an automated peptide synthesizer (Tribute-UV, Protein Technologies). All the coupling reactions were performed using HBTU coupling with 4 equivalents of the amino acid and 8% of diisoproylethylamine in DMF. For deprotection of Fmoc group, 25% v/v piperidine in DMF was used. Upon completion of synthesis of peptide on resin, compound **13d** was conjugated to the N-terminal of last amino acid using HBTU and DIPEA for 4h. To cleave the resin bound conjugated peptides, a cleavage mixture comprising of trifluoroacetic acid/thioanisole/phenol/ethanedithiol/H_2O (91.25:2.5:2.5:1.25:2.5) was used. Purification of the conjugated peptide was done on C-18 RP-HPLC column with linear gradients of water containing 0.1% TFA (gradient A) and acetonitrile containing 0.1% TFA (gradient B). The correct mass of each peptide after purification was characterized by LC-ESI-MS (Thermo Surveyor 355). Results of conjugate syntheses are summarized in Fig. S7.

#	Comp'	MIC_{90} (μM)
1	13c	86.6
2	13d	250
4	TAT	7.8
5	TAT conjugated 13d	1.9
6	Octaarginine	7.8
7	Octaarginine conjugated 13d	3.9
8	Isoniazid	250

Table 1. Anti- *Msmg* (mc^2155) activity of CPP conjugated dual acting inhibitor 13d.

Figures

Figure 1. Representation of the bacterial targets in this study: DNA primase and gyrase. a, Schematic representation of DNA priming system and DNA topoisomerase II in bacteria compared to their analogues in humans. Left: The DNA polymerase α–primase complex from human consists of four subunits. The p180 subunit is pol α, p58 and p49 comprise primase, and p68 is the fourth, accessory subunit. Right: structural differences between human and bacterial type II topoisomerases. **b**, Multiple sequence alignment of bacterial DnaG primase [*Aa- Aquifex aeolicus*, *Mtb-Mycobacterium tuberculosis*, *Sa-Staphylococcus aureus*, T7- bacteriophage T7]. Amino acid residues are colored from red for the most conserved amino acids to blue for the less conserved ones. **c,** Structural homology of the TOPRIM fold in Gyr and DnaG. Bacterial DnaG-like primases: T7 DNA primase (red, PDBID 1NUI [34]), part of the fused helicase-primase gp4 of bacteriophage T7, shares a similar structure with DnaG from *Mtb* (green, PDBID 5W33 [35]) and *S. aureus* (grey PDBID 4E2K[37]). *Mtb* Gyr (PDBID 3M4I) is presented in blue.

Figure 2. Inhibitory effect of synthesized molecules on DnaG primase and gyrase from *Mtb*. Screening for best precursor molecule among 18 commercially available compounds by examining their inhibitory effect on specific *Mtb* DnaG primase (template-directed ribonucleotide synthesis) and gyrase activity (ATPase activity and DNA-supercoiling). **a,** General scheme presents the template-directed ribonucleotide synthesis catalyzed by the primase. Reaction contained 500 nM *Mtb* DnaG primase, oligonucleotide (5'-CCGACCCGTCCGTAATACAGAGGTAATTGTCACGGT-3'), α-^{32}P-ATP, CTP, GTP, UTP and 4 mM of experimental inhibitor in the standard reaction mixture. After incubation, the radioactive products were analyzed by electrophoresis through a 25% polyacrylamide gel containing 7 M urea and visualized by autoradiography. Gel bands represent RNA primers formed by *Mtb* DnaG. **b,** General scheme showing the enzymatic activity of the Gyrase – catalysis of negative supercoiling of a plasmid by using the energy obtained by hydrolyzing two ATP molecules. Top: Inhibition of ATP hydrolysis by small molecule inhibitors. The 10 μL reaction containing DNA Gyr (reconstitution of 36 nM GyrA and 18 nM GyrB), 13.24 ng/μL pBR322 DNA and 38nM alpha-^{32}p-ATP in the presence of small molecule inhibitors was incubated at 37 °C for 60 min. The reaction was stopped using Norit solution (*see* Online Materials and Methods) and the radioactivity of the supernatant was determined. Bottom: Inhibition of DNA supercoiling by small molecule inhibitors. The reaction conditions were the same as described above. The reaction products were resolved in 1% agarose gel followed by staining with EtBr. **c,** distribution map of the effect of inhibitors on the

primase/Gyr activities. X-axis: inhibition of primase activity, y-axis: inhibition of ATPase activity of Gyr, z-axis: inhibition of Gyr supercoiling activity (circle size is proportional to magnitude of inhibition).

Figure 3. SAR- guided optimization of small molecule inhibitors for DnaG/GyrB of *Mtb*. **a,** Optimization of small molecule inhibitors was performed in three rounds of synthesis. Round I included development of indole derivatives (group I) viz. Indole diesters, Indole diacids, Indole dialcohols, Indole dicarboxaldehyde and Indole diamides. Round II included development of Indole derivatives (group II) viz. Indole monoesters and Indole monoacids. Round III included development of Indole derivatives (group III) viz. N-Benzylated Indole diesters, N-Benzylated Indole diacids, N-Benzylated Indole monoester and N-Benzylated Indole monoacid. **b,** Effect of newly synthesized small molecules on RNA primers synthesis catalyzed by DNA primase from *Mtb*. The reaction contained the oligonucleotide 5'-CCGACCCGTCCGTAATACAGAGGTAATTGTCACGGT-3', α-^{32}P-ATP, CTP, GTP, UTP in a standard reaction mixture, and 4 mM of each small molecule. The reaction was initiated by adding *Mtb* DnaG primase to a final concentration of 500 nM. After incubation, the radioactive products were analyzed by electrophoresis through a 25% polyacrylamide gel containing 7 M urea, and visualized using autoradiography.
c, Effect of newly synthesized small molecules on Gyr activity. Top: Inhibition of ATP hydrolysis by small molecule inhibitors. Bottom: Inhibition of DNA supercoiling by small molecule inhibitors. The experiment was performed as described in Fig. 2b. **d,** Scheme of synthesis of derivative compounds based on SAR conclusions. Group 1) a. Electron withdrawing group (e.g., NO_2, CF_3, Cl) renders phenyl ring less nucleophilic and thus more likely to support activity. Incorporation of electron releasing group (e.g., CH_3, OH) hinders activity. b. Bulky groups introduce steric hindrance and decrease activity. c. Indole ring. Five membered nitrogen heterocyclic ring system is essential for activity. d. Free nitrogen is essential for activity. Lone pair located on the nitrogen atom is in resonance, and therefore, it stabilizes the structure. e. Carboxylate ester is essential for activity. Activity is reduced when modified to alcohols, amides, aldehydes but increased upon conversion to acid. Group 2) f. Carboxyl group is essential. Activity is reduced when modified to ester, alcohols, amides, aldehydes. Group 3) g. Utilization of free –NH linkage of Indole. Substituting the –H of –NH of Indole with benzyl group increases the inhibition. **e,** Correlation of enzymatic activities in the presence of derivative molecules. X-axis: inhibition of primase activity, y-axis: inhibition of ATPase activity of Gyr, z-axis: inhibition of Gyr supercoiling activity (circle size is proportional to magnitude of inhibition).

Figure 4. Effect of selected small molecule inhibitors *on Msmg* culture growth. a, Growth curves of *Msmg* culture expressing mCherry reporter protein. The culture was grown in 7H9 liquid medium (0.4% glycerol, 0.05% Tween-80) containing different small molecule inhibitors in 250 μM concentration. The fluorescent signal originating form mCherry reporter protein was measured over the course of 20 hours and used to estimate viability of bacterial cells. Data represents the average of three replicates (n=3). Inset shows the effect of compounds **13c** and **13d** on the viability of *Msmg* (compared to isoniazid, INH, indicated in grey). **b,** Dilution colony assay. Samples from the assay described in **a** were collected after incubation and serially diluted in 1:10 ratio. Each dilution was platted on a 7H10+ agar plate and incubated until bacterial colonies became visible. **c,** Chemical structure of transactivator of transcription (TAT) peptide of human immunodeficiency virus (cell penetrating peptide) and octaarginine conjugated to the inhibitor **13d**.

Figure 5. Inhibition/eradication of biofilm by primase/gyr inhibitors. a, Inhibition of biofilm growth of *Msmg* mc^2155 by various concentrations of selected inhibitors. Top: Alamar blue viability assay of biofilm-embedded bacteria after treatment with selected inhibitors and their conjugates. Middle: growth measurements. Bottom: optical image of five days old *Msmg* biofilm grown on polystyrene plate, where, A1-negative control, A2-DMSO vehicle control 1.2%, A3-DMSO 0.62%, A4-DMSO 0.31%, B1- **13c** (250μM), B2-**13c** (125 μM), B3-**13d** (250μM), B4-**13d** (125 μM), C1-**13d**-conjugated to cell penetrating peptide (**13d-CPP**, 2μM), C2-**13d-CPP** (1μM), C3-CPP only (8μM), C4-CPP only (4μM), D1-Isoniazid (INH, 250μM), D2-INH (125μM), D3-4-positive control. **b,** Eradication of preformed biofilm of *Msmg* mc^2155. Top: Alamar blue viability assay of preformed biofilm after treatment with selected inhibitors and their conjugates. Middle: growth measurements. Bottom: optical image of five days old *Msmg* biofilm grown on polystyrene plate, where, A1-2-negative control, A3-DMSO 1.2%, A4-DMSO 0.62%, B1- **13c** (250μM), B2-**13c** (125 μM), B3-**13d** (250μM), B4-**13d** (125 μM), C1-**13d-CPP** (2μM), C2-**13d-CPP** (1μM), C3-CPP only (8μM), C4-CPP only (4μM), D1-Isoniazid (INH, 250μM), D2-INH (125μM), D3-4-positive control.

Figure 6. Summary of binding-activity cliff studies on compounds 10c and 10d and their corresponding analogues 13c and 13d. Color coding is used to highlight functional regions of the lead compounds. Changes in region A of compound **10c** and **10d** are shown in blue, changes in region B are shown in red, and changes in region C are shown in green.

Acknowledgments

This work was supported by grants from the Bi-National Science Foundation (BSF, grant number 2016142), the ISRAEL SCIENCE FOUNDATION (grant No. 1023/18), and the IMTI (TAMAT) / Israel Ministry of Industry– KAMIN Program, Grant No. 59081. We thank Prof. Jack Cohen (BGU) for helpful discussions and Prof. Gonen Ashkenazy for help in peptide synthesis.

References

1. Udwadia, Z.F., Amale, R.A., Ajbani, K.K. & Rodrigues, C. Totally drug-resistant tuberculosis in India. *Clin Infect Dis* **54**, 579-81 (2012).
2. Ashley, R.E. et al. Activities of gyrase and topoisomerase IV on positively supercoiled DNA. *Nucleic Acids Res* **45**, 9611-9624 (2017).
3. Morais Cabral, J.H. et al. Crystal structure of the breakage-reunion domain of DNA gyrase. *Nature* **388**, 903-6 (1997).
4. Ilic, S. et al. DnaG Primase-A Target for the Development of Novel Antibacterial Agents. *Antibiotics (Basel)* **7**(2018).
5. Aravind, L., Leipe, D.D. & Koonin, E.V. Toprim--a conserved catalytic domain in type IA and II topoisomerases, DnaG-type primases, OLD family nucleases and RecR proteins. *Nucleic Acids Res* **26**, 4205-13 (1998).
6. Strack, B., Lessl, M., Calendar, R. & Lanka, E. A common sequence motif, -E-G-Y-A-T-A-, identified within the primase domains of plasmid-encoded I- and P-type DNA primases and the alpha protein of the Escherichia coli satellite phage P4. *J Biol Chem* **267**, 13062-72 (1992).
7. Chen, S.J. & Wang, J.C. Identification of active site residues in Escherichia coli DNA topoisomerase I. *J Biol Chem* **273**, 6050-6 (1998).
8. Wigley, D.B., Davies, G.J., Dodson, E.J., Maxwell, A. & Dodson, G. Crystal structure of an N-terminal fragment of the DNA gyrase B protein. *Nature* **351**, 624-9 (1991).
9. Maxwell, A. The interaction between coumarin drugs and DNA gyrase. *Mol Microbiol* **9**, 681-6 (1993).
10. Hooper, D.C. Mode of action of fluoroquinolones. *Drugs* **58 Suppl 2**, 6-10 (1999).
11. Mdluli, K. & Ma, Z. Mycobacterium tuberculosis DNA gyrase as a target for drug discovery. *Infect Disord Drug Targets* **7**, 159-68 (2007).
12. Gellert, M., O'Dea, M.H., Itoh, T. & Tomizawa, J. Novobiocin and coumermycin inhibit DNA supercoiling catalyzed by DNA gyrase. *Proc Natl Acad Sci U S A* **73**, 4474-8 (1976).
13. Alt, S., Mitchenall, L.A., Maxwell, A. & Heide, L. Inhibition of DNA gyrase and DNA topoisomerase IV of Staphylococcus aureus and Escherichia coli by aminocoumarin antibiotics. *J Antimicrob Chemother* **66**, 2061-9 (2011).
14. Zignol, M. et al. Population-based resistance of Mycobacterium tuberculosis isolates to pyrazinamide and fluoroquinolones: results from a multicountry surveillance project. *Lancet Infect Dis* **16**, 1185-1192 (2016).
15. Connolly, L.E., Edelstein, P.H. & Ramakrishnan, L. Why is long-term therapy required to cure tuberculosis? *PLoS Med* **4**, e120 (2007).
16. Hett, E.C. & Rubin, E.J. Bacterial growth and cell division: a mycobacterial perspective. *Microbiol Mol Biol Rev* **72**, 126-56, table of contents (2008).
17. Rani, S.A. et al. Spatial patterns of DNA replication, protein synthesis, and oxygen concentration within bacterial biofilms reveal diverse physiological states. *J Bacteriol* **189**, 4223-33 (2007).
18. Esteban, J. & Garcia-Coca, M. Mycobacterium Biofilms. *Front Microbiol* **8**, 2651 (2017).

19. Teng, R. & Dick, T. Isoniazid resistance of exponentially growing Mycobacterium smegmatis biofilm culture. *FEMS Microbiol Lett* **227**, 171-4 (2003).
20. Singh, M., Tam, B. & Akabayov, B. NMR-Fragment Based Virtual Screening: A Brief Overview. *Molecules* **23**(2018).
21. Ilic, S. et al. Identification of DNA primase inhibitors via a combined fragment-based and virtual screening. *Sci Rep* **6**, 36322 (2016).
22. Chilingaryan, Z. et al. Fragment-Based Discovery of Inhibitors of the Bacterial DnaG-SSB Interaction. *Antibiotics (Basel)* **7**(2018).
23. Akladios, F.N. et al. Design and synthesis of novel inhibitors of human kynurenine aminotransferase-I. *Bioorg Med Chem Lett* **22**, 1579-81 (2012).
24. Bie, J. et al. Discovery of novel indole derivatives as allosteric inhibitors of fructose-1,6-bisphosphatase. *Eur J Med Chem* **90**, 394-405 (2015).
25. Gengenbacher, M. & Kaufmann, S.H. Mycobacterium tuberculosis: success through dormancy. *FEMS Microbiol Rev* **36**, 514-32 (2012).
26. Gorla, P. et al. MtrA Response Regulator Controls Cell Division and Cell Wall Metabolism and Affects Susceptibility of Mycobacteria to the First Line Antituberculosis Drugs. *Front Microbiol* **9**, 2839 (2018).
27. Futaki, S. Membrane-permeable arginine-rich peptides and the translocation mechanisms. *Adv Drug Deliv Rev* **57**, 547-58 (2005).
28. Lindgren, M., Hallbrink, M., Prochiantz, A. & Langel, U. Cell-penetrating peptides. *Trends Pharmacol Sci* **21**, 99-103 (2000).
29. Wadia, J.S. & Dowdy, S.F. Transmembrane delivery of protein and peptide drugs by TAT-mediated transduction in the treatment of cancer. *Adv Drug Deliv Rev* **57**, 579-96 (2005).
30. Sparr, C. et al. Improved efficacy of fosmidomycin against Plasmodium and Mycobacterium species by combination with the cell-penetrating peptide octaarginine. *Antimicrob Agents Chemother* **57**, 4689-98 (2013).
31. Gotoh, H. et al. Pseudomonas aeruginosa, under DNA replication inhibition, tends to form biofilms via Arr. *Res Microbiol* **159**, 294-302 (2008).
32. Anand, A. et al. Polyketide Quinones Are Alternate Intermediate Electron Carriers during Mycobacterial Respiration in Oxygen-Deficient Niches. *Mol Cell* **60**, 637-50 (2015).
33. Trivedi, A., Mavi, P.S., Bhatt, D. & Kumar, A. Thiol reductive stress induces cellulose-anchored biofilm formation in Mycobacterium tuberculosis. *Nat Commun* **7**, 11392 (2016).
34. Kato, M., Ito, T., Wagner, G., Richardson, C.C. & Ellenberger, T. Modular architecture of the bacteriophage T7 primase couples RNA primer synthesis to DNA synthesis. *Mol Cell* **11**, 1349-60 (2003).
35. Hou, C., Biswas, T. & Tsodikov, O.V. Structures of the Catalytic Domain of Bacterial Primase DnaG in Complexes with DNA Provide Insight into Key Priming Events. *Biochemistry* **57**, 2084-2093 (2018).
36. Morris, G.M. et al. AutoDock4 and AutoDockTools4: Automated docking with selective receptor flexibility. *J Comput Chem* **30**, 2785-91 (2009).
37. Rymer, R.U. et al. Binding mechanism of metalNTP substrates and stringent-response alarmones to bacterial DnaG-type primases. *Structure* **20**, 1478-89 (2012).

Figure 1

a.

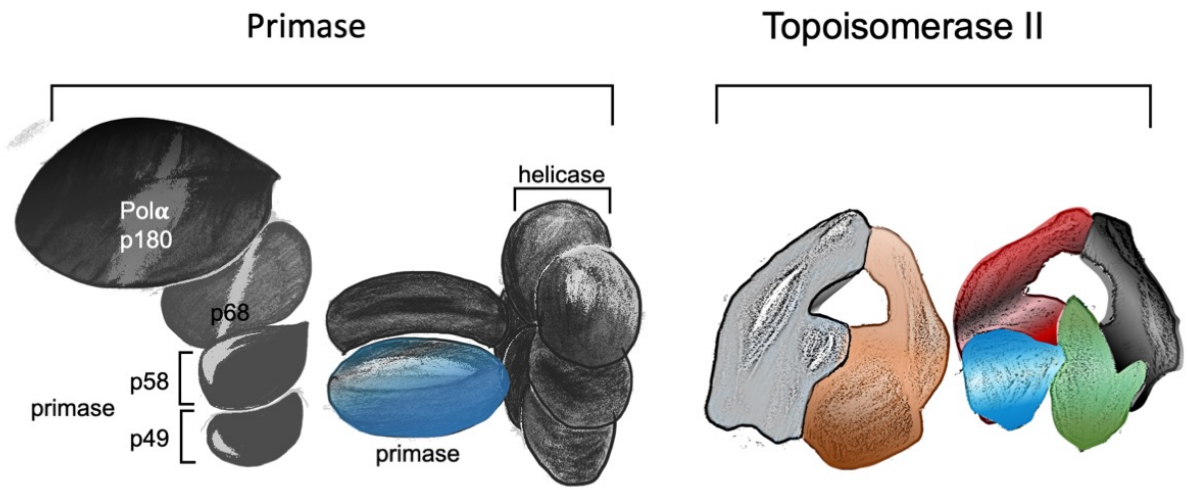

b.

```
Aa DnaG     E-GFAILVEGYF--DLLR-LFSEGIRNVVAPL-GTALTQNQANL--LSK-------FTKKVYIL
Mtb DnaG    G-HQAVVVEGYT--DVMA-MHLAGVTTAVASC-GTAFGGEHLAM--LRRLMMDDSFFRGELIYV
Sa DnaG     KLDEIVLLEGFM--DVIK-SDTAGLKNVVATM-GTQLSDEHITF--IRK-------LTSNITLM
Mtb GyrB    K-SELYVVEGDSAGGSAK-SGRDSMFQAILPLRGKIINVEKARIDRVLKNTEVQAIITALGTGI
T7 primase  G-KKIVVTEGEI--DMLTVMELQDCKYPVVSL-GHGASAAKKTCAANYEYFD----QFEQIILM

Aa DnaG     YDGDDAGR----KAMKSAIPLLLSAGVEVYPVYL------P---EGY----DPDEFIKEFGKEE
Mtb DnaG    FDGDEAGR----AAALKAFDGEQKLAGQSFVAVA------P---DGM----DPCDLRLKCGDAA
Sa DnaG     FDGDFAGS----EATLKTGQNLLQQGLNVFVIQL------P---SGM----DPDEYIGKYGNDA
Mtb GyrB    HDEFDIGKLRYHKIVLMADADVDGQHISTLLLTLLFRFMRPLIENGHVFLAQPPLYKLKWQRSD
T7 primase  FDMDEAGR----KAVEEAAQVLPAGKVRVAVLPC-------KDAN----ECHLNGHDREIME
```

c.

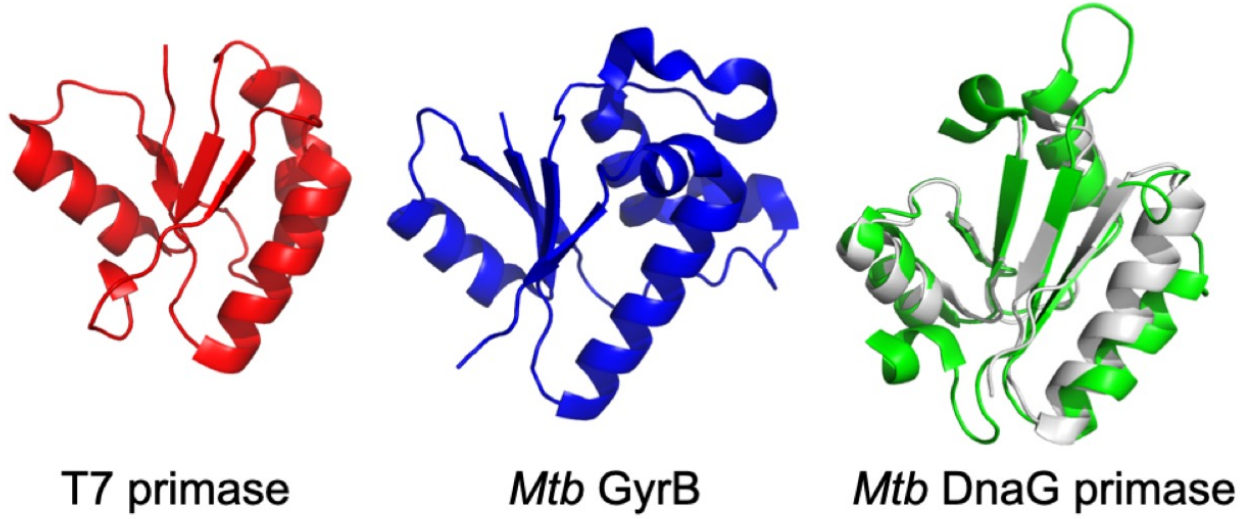

Figure 2

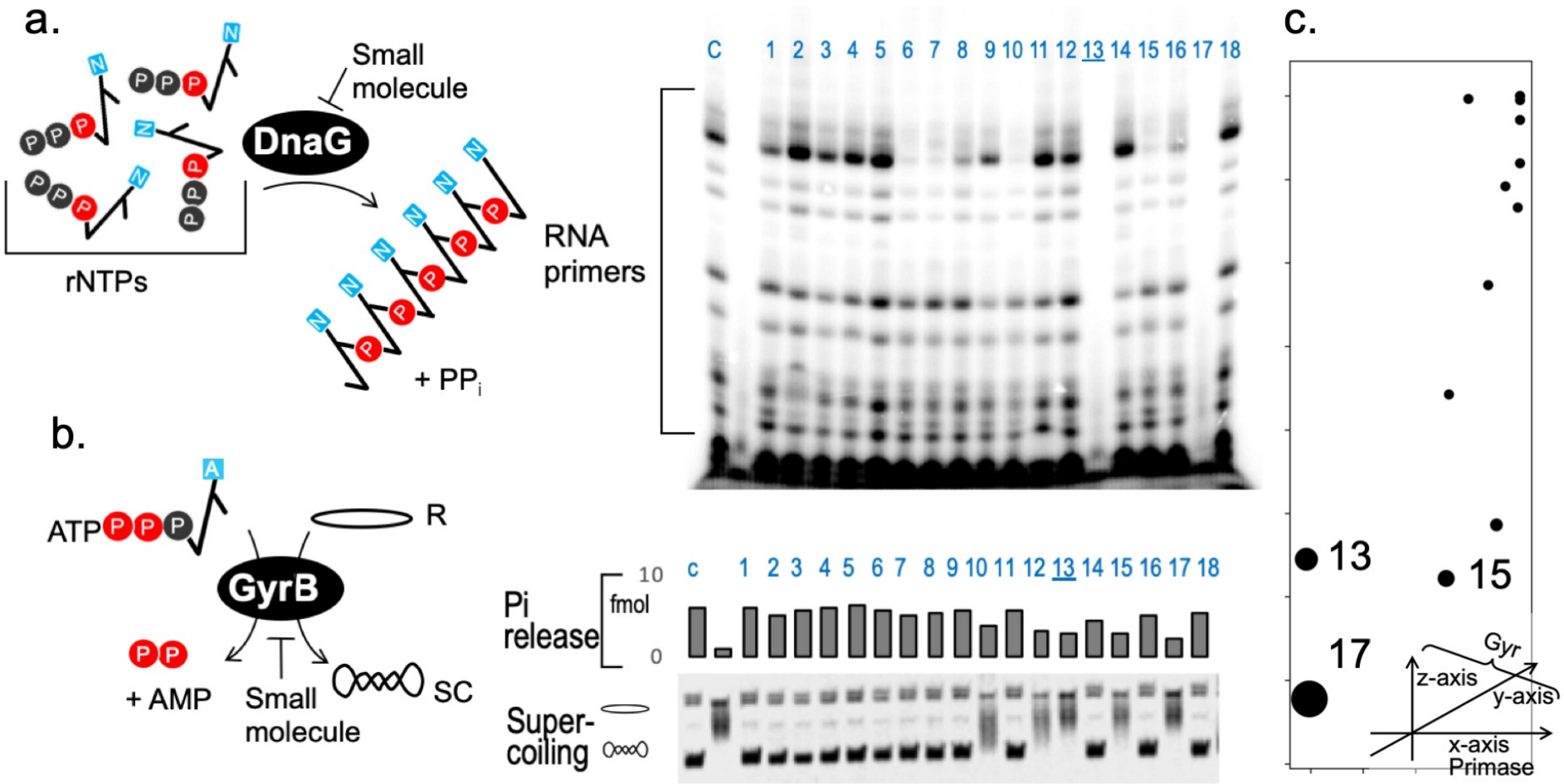
a.
Small molecule
DnaG
rNTPs
RNA primers
+ PPi
b.
ATP
R
GyrB
+ AMP
Small molecule
SC
c. 1 2 3 4 5 6 7 8 9 10 11 12 13 14 15 16 17 18
Pi release
10 fmol
0
Super-coiling
13
15
17
Gyr
z-axis
y-axis
x-axis
Primase

Figure 3

a.

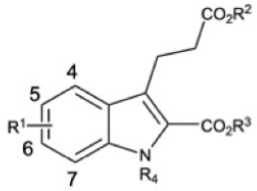

b.

#	R^1	R^2	R^3	R^4
3a	5-Cl	Et	Et	H
3b	5-NO_2	Et	Et	H
3c	5-Cl, 4-CF_3	Et	Et	H
3c'	5-Cl, 6-CF_3	Et	Et	H
3d	7-Cl, 5-CF_3	Et	Et	H
3e	4,7-diCl, 5-NO_2	Et	Et	H
3f	4,6-diCF_3	Et	Et	H
3g	5-CH_3	Et	Et	H
6a	5-Cl	H	H	H
6b	5-NO_2	H	H	H
6c	5-Cl, 4-CF_3	H	H	H
6c'	5-Cl, 6-CF_3	H	H	H
6d	7-Cl, 5-CF_3	H	H	H
6e	4,7-diCl, 5-NO_2	H	H	H
6f	4,6-diCF_3	H	H	H
6g	5-CH_3	H	H	H

#	R^1	R^2	R^3	R^4
8b	5-NO_2	Et	H	H
8c	5-Cl, 4-CF_3	Et	H	H
8c'	5-Cl, 6-CF_3	Et	H	H
8d	7-Cl, 5-CF_3	Et	H	H
8f	4,6-diCF_3	Et	H	H
9a	5-Cl	H	Et	H
9b	5-NO_2	H	Et	H
9c	5-Cl, 4-CF_3	H	Et	H
9c'	5-Cl, 6-CF_3	H	Et	H
9d	7-Cl, 5-CF_3	H	Et	H
9e	4,7-diCl, 5-NO_2	H	Et	H
9f	4,6-diCF_3	H	Et	H

#	R^1	R^2	R^3	R^4
10a	5-Cl	Et	Et	Bn
10b	5-NO_2	Et	Et	Bn
10c	5-Cl, 4-CF_3	Et	Et	Bn
10c'	5-Cl, 6-CF_3	Et	Et	Bn
10d	7-Cl, 5-CF_3	Et	Et	Bn
10e	4,7-diCl, 5-NO_2	Et	Et	Bn
10f	4,6-diCF_3	Et	Et	Bn
10g	5-CH_3	Et	Et	Bn
11a	5-Cl	H	H	Bn
11b	5-NO_2	H	H	Bn
11c'	5-Cl, 6-CF_3	H	H	Bn
11d	7-Cl, 5-CF_3	H	H	Bn

4a: R^5 = CH_2OH
5a: R^5 = CHO
7a: R^5 = CONHPh

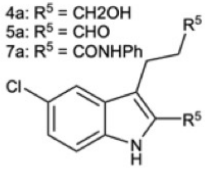

#	R^1	R^2	R^3	R^4
12a	5-Cl	Et	H	Bn
12b	5-NO_2	Et	H	Bn
12c	5-Cl, 4-CF_3	Et	H	Bn
12c'	5-Cl, 6-CF_3	Et	H	Bn
13a	5-Cl	H	Et	Bn
13b	5-NO_2	H	Et	Bn
13c	5-Cl, 4-CF_3	H	Et	Bn
13c'	5-Cl, 6-CF_3	H	Et	Bn
13d	7-Cl, 5-CF_3	H	Et	Bn

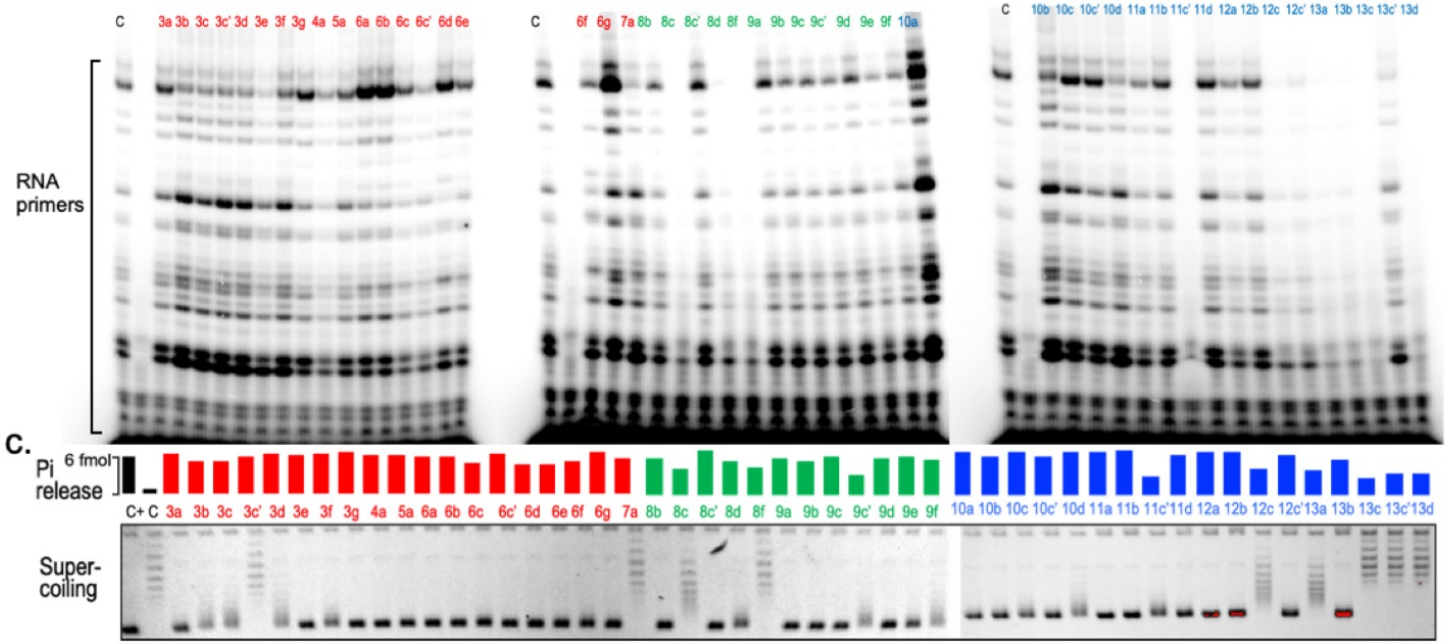

d.

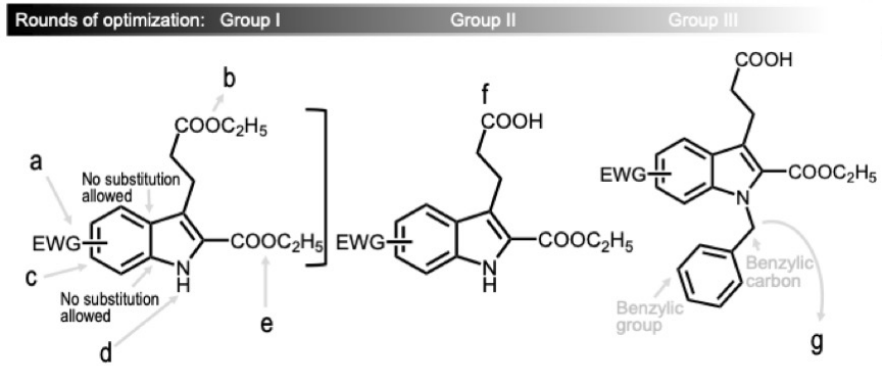

e.

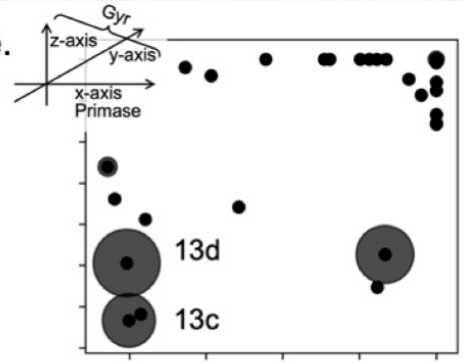

Figure 4

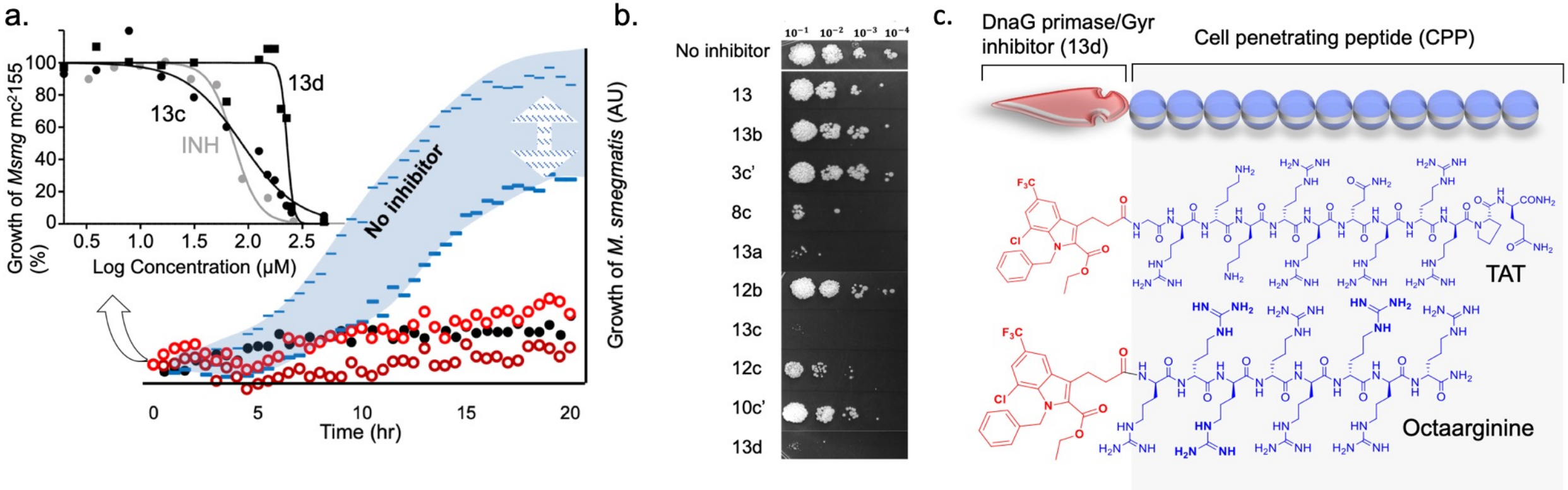
a.
Growth of Msmg mc²155 (%)
100
80
60
40
20
0
0.5
1.0
1.5
2.0
2.5
Log Concentration (μM)
13d
13c
INH
No inhibitor
0
5
10
15
20
Time (hr)
Growth of M. smegmatis (AU)
b.
10⁻¹ 10⁻² 10⁻³ 10⁻⁴
No inhibitor
13
13b
3c'
8c
13a
12b
13c
12c
10c'
13d
c.
DnaG primase/Gyr inhibitor (13d)
Cell penetrating peptide (CPP)
TAT
Octaarginine

Figure 5

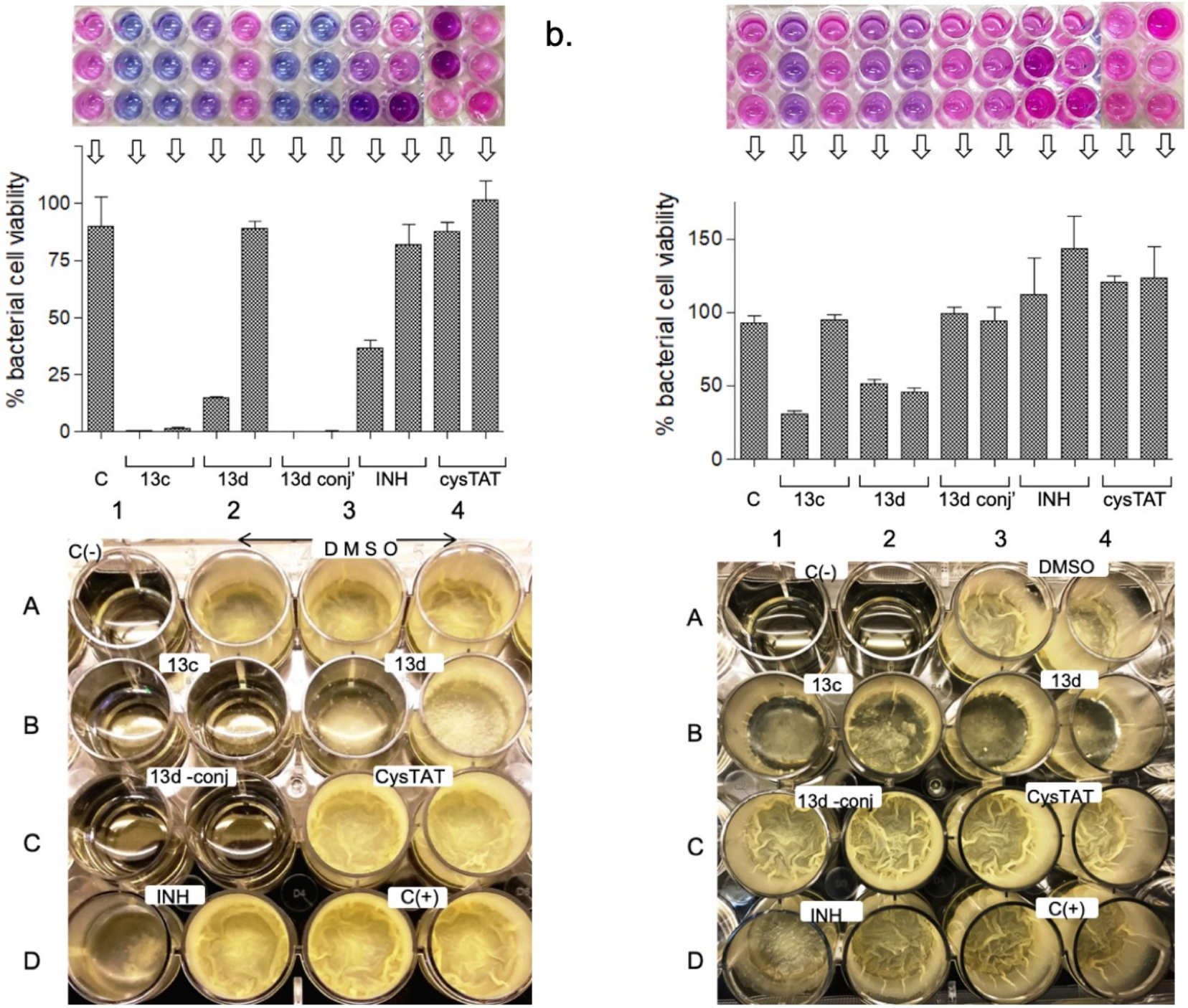
a.
b.
% bacterial cell viability
100
75
50
25
0
150
C
13c
13d
13d conj'
INH
cysTAT
1
2
3
4
C(-)
D M S O
DMSO
A
B
C
D
13c
13d
13d -conj
CysTAT
INH
C(+)

Figure 6

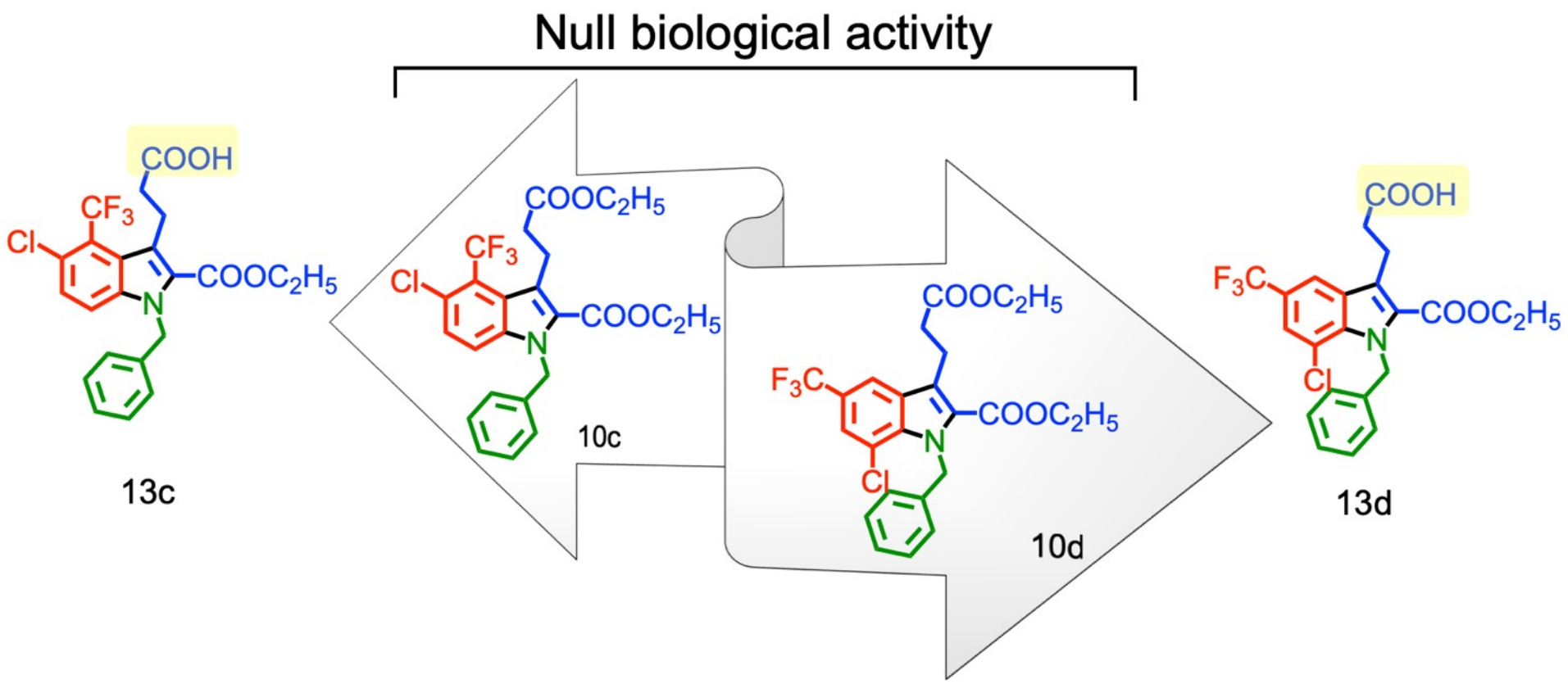
Null biological activity
COOH
CF3
Cl
COOC2H5
N
13c
COOC2H5
CF3
Cl
COOC2H5
N
10c
COOC2H5
F3C
COOC2H5
N
Cl
10d
COOH
F3C
COOC2H5
N
Cl
13d